Stimulated Emission Pumping Spectra and Intramolecular Vibrational Dynamics of DFCO(S_0) from 9000 to 20 000 cm^{-1}

Jason C. Crane,[†] Hakhyun Nam,[‡] Horst Clauberg,[§] Harry P. Beal,[||] Ilia J. Kalinovski, Richard G. Shu, and C. Bradley Moore*

Department of Chemistry, University of California at Berkeley, Berkeley, California 94720-1460

Received: April 20, 1998; In Final Form: July 8, 1998

Dispersed fluorescence (DF) and stimulated emission pumping (SEP) spectra of DFCO from 9000 to 20 000 cm^{-1} on S_0 are reported. Groups of features in the $2^1 5^1 6^2$ DF spectrum are assigned as strongly coupled members of 266 [ν_2(CO stretch) ↔ $2\nu_6$(out-of-plane bend)] polyads of vibrational states. The Franck−Condon active states in these polyads are primarily the zero-order states $2_n 6_m$ with values of n ranging from 0 to 4 and values of m ranging from 13 to 19. The assignment of the Franck−Condon active states is consistent with the HFCO experimental results and with Franck−Condon factor calculations. Multiple intramolecular vibrational energy redistribution (IVR) time scales are evident from the dilution of the Franck−Condon factors observed in the spectra examined at different resolutions. The fastest IVR results from the low-order (Δv = 3) 266 resonance that couples ν_2 and ν_6. This initial IVR occurs in ∼25 fs. Evidence of anharmonic coupling within the vicinity of single DF features signifies subsequent IVR on the 0.5−4.0 ps time scale. This second time scale can be understood in terms of further coupling to ν_3 (HCO bend) and ν_5 (FCO bend) resulting from a 3566 Darling−Dennison resonance. Clumps of vibrational lines within individual SEP bands indicate further anharmonic and weak A-type Coriolis coupling to background levels at times between 3 and 150 ps. Comparison of the observed and calculated vibrational-state densities indicates that, for many states, IVR may be nearly complete on the time scale of the measured dissociation rates. The IVR dynamics of DFCO are in marked contrast to the mode-specific IVR dynamics of HFCO. The quasistability of extreme-motion out-of-plane vibrations ($v_6 \geq 14$), in HFCO is destroyed by the strong coupling of ν_2 and $2\nu_6$ in DFCO. Thus, the two isotopomers display qualitatively different IVR dynamics.

I. Introduction

The idea that vibrational energy is randomized rapidly on the time scale of a chemical reaction is the underlying assumption of statistical unimolecular reaction rate theories such as RRKM.[1−5] Consequently, these theories give dissociation rates that are insensitive to the initial vibrational excitation and depend only on total energy and angular momentum. The success of these theories at predicting the rates of thermal reactions supports this assumption,[5] yet state-selective studies of unimolecular dissociation have revealed evidence for incomplete intramolecular vibrational energy redistribution (IVR) as well as for both mode- and state-specific dynamics. Analysis of statistical properties such as level spacing and dissociation rate distributions of CH_3O below 10 000 cm^{-1},[6] D_2CO near 28 000 cm^{-1},[7,8] and C_2H_2 near 27 900 cm^{-1} [9] do indicate complete IVR. Nevertheless, the dynamics of D_2CO exhibit state-specific fluctuations resulting from the random distribution of the wave function coefficients in a strongly mixed system. Due to Coriolis-induced vibrational coupling, the dissociation rates of HFCO depend strongly and systematically on the rotational quantum numbers.[10] The relative time scales of IVR and dissociation are critical factors that determine the relation between the initially excited state and the reaction outcome. Thus, it is desirable to understand and be able to predict the coupling mechanisms responsible for IVR as well as the time scale and extent of IVR in polyatomic molecules. A thorough understanding of IVR will allow a prediction of when dynamics will be statistical vs mode specific and will aid in the development of reaction rate theories that account for and predict dissociation dynamics in nonstatistical systems.

Much of the current understanding of IVR is a result of frequency domain spectral studies. The signature of IVR in the frequency domain is the perturbation and dilution of zero-order optically active states that result from anharmonic or Coriolis coupling to optically dark states.[11−13] IVR has been studied in fundamental vibrations[14,15] as well as in highly vibrationally excited dissociative systems.[16] Despite the success of the normal mode picture of independent harmonic oscillators for describing vibrations near the bottom of the potential-energy surface (PES), extensive IVR has been observed for CH-stretching fundamentals[14] and low overtones.[15] Additionally, instances of slow and incomplete IVR have been observed in highly vibrationally excited systems where the PES is quite anharmonic and state densities are high. For example, in HFCO at dissociative energies, states with all of the vibrational energy in ν_6 (see Table 1), so-called extreme-motion states, are particularly stable against IVR.[16] IVR increases, in a mode-specific way, for isoenergetic states with more excitation in ν_2 and correspondingly less excitation in ν_6. Although high state densities do increase the likelihood of vibrational couplings and

[†] Current address: Beckman Institute for Advanced Science and Technology and Department of Chemistry, University of Illinois, Urbana, IL 61801.

[‡] Current address: Department of Chemistry, Kwangwoon University, Seoul 139-701, Korea.

[§] Current address: Eastman Chemical Co., Kingsport, TN 37662.

[||] Current address: Anderson Consulting, San Francisco, CA 94105.

10.1021/jp981917b CCC: $15.00
Published on Web 09/12/1998

TABLE 1: HFCO and DFCO S_0 Fundamental Frequencies (cm^{-1})

	HFCO[16]	DFCO[21]
ν_1 A′ (CD stretch)	2981	2262
ν_2 A′ (CO stretch)	1837	1797
ν_3 A′ (DCO bend)	1343	968
ν_4 A′ (CF stretch)	1065	1073
ν_5 A′ (FCO bend)	663	658
ν_6 A″ (out-of-plane bend)	1011	857

IVR, evidence suggests that it is the density of low-order resonances ($\Delta v = 3-4$) that is crucial.[13,17−19] For example, vibrational couplings evident in the $5\nu_{OH}$ spectrum of CH_3OH vary by a factor of 5 over only a 50 cm^{-1} range, suggesting that specific lower-order resonances, rather than the total state density, control the vibrational dynamics.[19] Additionally, the stability of extreme-motion states against IVR is predicted due to the reduced number of low-order couplings between these states and isoenergetic bath states.[20] Low-order resonances depend on the ratios of the vibrational frequencies, and, thus, can be turned on and off by isotopic substitution without changing the PES or significantly affecting the total state density. Thus, the question of the relative importance of low- vs high-order resonances is directly addressed by comparison of the IVR dynamics in HFCO and DFCO.

The spectrum of DFCO at dissociative energies is significantly more complex than the HFCO spectrum at comparable energies. Thus, the DFCO spectrum was first analyzed at S_0 energies below 9000 cm^{-1}.[21] Spectroscopic constants were obtained, and several strong anharmonic resonances were identified that, due to differences in vibrational frequencies, are not important for HFCO. The current work presents the continued analysis of the SEP spectra and intramolecular vibrational dynamics of DFCO between 9000 and 20 000 cm^{-1}. Characterization of the dissociative states is essential for the interpretation of state-selective rate measurements currently underway in this group. Additionally, the results of this analysis provide a strong test for the quality of ab initio formyl fluoride force fields.[22−28] Experiments and spectra are presented in sections II and III, respectively. In section IV, Franck−Condon active zero-order states are identified. Evidence is presented for anharmonic and Coriolis coupling in DFCO over multiple time scales in section V. In section VI, experimental and calculated state densities are compared to determine the extent of IVR on the time scale of the unimolecular dissociation reaction.

II. Experimental Section

The experimental procedures have been described previously[21,29] and are reviewed here briefly. Jet-cooled DFCO is excited to rovibrational levels of S_1 with pulses generated by frequency doubling, in a β-bariumborate (BBO) crystal, the output of a dye laser (Lambda Physik Fl2002, $\Delta\nu = 0.15$ cm^{-1}) pumped by the third harmonic of a Nd:YAG laser (Quantel YG580). There was 99.6% of the fundamental (10−15 mJ/pulse) separated from the frequency-doubled light (1.0−1.5 mJ/pulse) by three dichroic mirrors before the UV enters the molecular beam chamber. The laser crosses the pulsed molecular beam approximately 2 cm from the nozzle. The polarization of the laser is fixed in the vertical plane formed by the laser and molecular beam.

$S_1 \rightarrow S_0$ dispersed fluorescence (DF) spectra were recorded from the ^rQ subband heads of the $2^15^16^2$ (39 779.2 cm^{-1}) and 5^16^6 (39 952.4 cm^{-1}) vibrational levels of S_1. Fluorescence emitted perpendicular to the plane formed by the laser and molecular beams is dispersed in a 75 cm monochromator (Spex 1700) with a 1200 groove/mm grating blazed at 500 nm. The monochromator entrance slit and the grating grooves are oriented parallel to the polarization of the laser beam. Dispersed fluorescence is detected with a PMT (Hamamatsu H1161) and integrated with a boxcar integrator (SRS model 250). The resolution of the monochromator, operated in first order with a slit width of 0.5 mm, is ∼90 cm^{-1}. The monochromator is calibrated with a Hg and Kr lamp to ±5 cm^{-1}.

Stimulated emission pumping (SEP) spectra were recorded from the completely resolved 1_{10} rotational levels of the 5^16^4 (39 388.72 cm^{-1}), 6^6 (39 523.92 cm^{-1}), 2^2 (39 679.72 cm^{-1}), $2^15^16^2$ (39 780.23 cm^{-1}), 5^26^4 (39 823.40 cm^{-1}), 5^16^6 (39 953.38 cm^{-1}), 2^16^4 (40 006.78 cm^{-1}), and $2^13^16^2$ (40 218.16 cm^{-1}) S_1 vibrational states. Pump light is produced as described above with the exception that the dye laser is fit with an intracavity Etalon narrowing the bandwidth to $\Delta\nu \leq 0.05$ cm^{-1}. The output (6−20 mJ/pulse) of another Nd:YAG (Quanta Ray DCR 1A) pumped dye laser (Lambda Physik FL3002, $\Delta\nu \leq 0.15$ cm^{-1} ($\Delta\nu \leq 0.05$ cm^{-1} with intracavity Etalon)) stimulates emission back to S_0 following a 25−100 ns delay, chosen to be approximately 20% of the S_1 fluorescence lifetime. $S_1 \rightarrow S_0$ fluorescence is collected with a PMT (Hamamatsu H1161) mounted perpendicular to the plane formed by the laser beam and molecular beam. A color filter (Schott BG-25, transmits $\lambda \geq 280$ nm) and a dielectric mirror ($R_{max} = 250$ nm) are placed in front of the PMT to reduce the amount of scattered light detected.

SEP transitions are detected as a decrease in the fluorescence signal integrated (SRS boxcar integrator model 250) during a 400 ns gate opened immediately after the interaction of the dump laser with the molecular beam. Spectra are normalized for fluctuations in the number of excited molecules.[16] These fluctuations are detected as variations in the integrated fluorescence signal from an identical boxcar integrator opened during the 25−100 ns separation between the pump and dump pulses.

Pump frequencies are calibrated to ±0.02 cm^{-1} with a Burleigh WA-4500 wavemeter. Fe/Ne optogalvanic spectra are recorded during SEP scans for absolute calibration of dump frequencies to ±0.3 cm^{-1}.[30] Absolute S_0 frequencies above the zero-point energy are taken as the difference between the excitation frequency and the dump frequency and are accurate to ±0.3 cm^{-1}.

DFCO is synthesized from deuterated formic acid and cyanuric fluoride using the method of Olah et al. [31] Following synthesis, the sample is vacuum distilled from 193 (CO_2(s) and acetone slush) to 77 K (N_2(l)) to remove impurities. The sample is stored at 77 K when not in use.

III. Spectra

DF spectra of DFCO, extending from 9000 to 20 000 cm^{-1} on S_0, are shown in Figure 1. Fluorescence originates from the ^rQ subband heads of the $2^15^16^2$ and 5^16^6 vibrational levels of S_1. Several characteristics of the DF spectra are noteworthy. First, well-resolved transitions to states above the dissociation barrier (17 200 ±1400 cm^{-1} [10]) are observed in both spectra. Thus, SEP can be used to excite DFCO to dissociative S_0 states. The $2^15^16^2$ spectrum is fairly congested between 9000 and 10 500 cm^{-1}. At higher energies, groups of DF peaks are observed that are separated by regions of lesser intensity. These groups consist of two or three relatively intense DF peaks within a 200 cm^{-1} window. For example, the DF peaks near 15 600, 15 700, and 15 800 cm^{-1} in the $2^15^16^2$ spectrum (Figure 1)

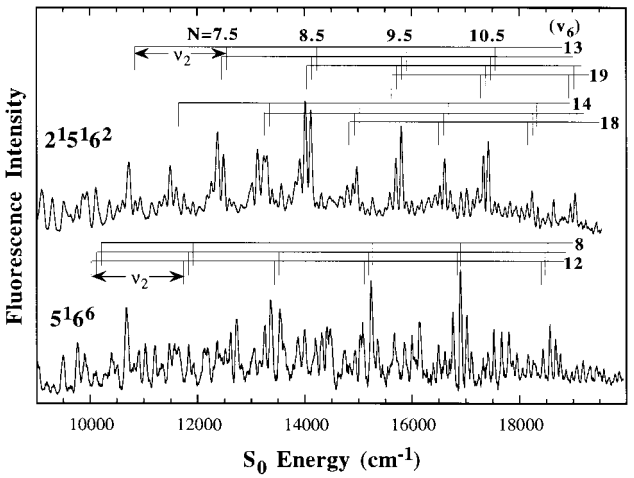

Figure 1. Dispersed fluorescence spectra of DFCO recorded from the ^rQ subband heads of the $2^15^16^2$ and 5^16^6 vibrational levels of S_1. Progressions in ν_2 are shown for the zero-order states 2_n6_m for $n = 0-4$ and $m = 13-19$ (top). In the 5^16^6 spectrum, the 2_n6_8, 2_n6_{10}, and 2_n6_{12} progressions are labeled for $n = 2-7$, $n = 1-6$, and $n = 0-5$, respectively. Polyad numbers, $N = \nu_2 + \nu_6/2$, are indicated for several A″ polyads.

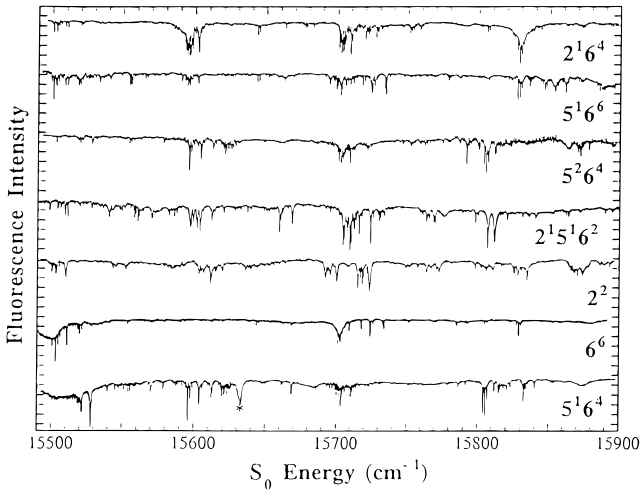

Figure 2. SEP spectra in the vicinity of the features near 15 800 cm^{-1} in the $2^15^16^2$ DF spectrum shown in Figure 1. All spectra were recorded at low ($\Delta\nu \leq 0.15$ cm^{-1}) resolution and perpendicular polarization with the exception of the $2^15^16^2$ spectrum, which was recorded with parallel polarization. The asterisk in the 5^16^4 spectrum indicates an upward transition.

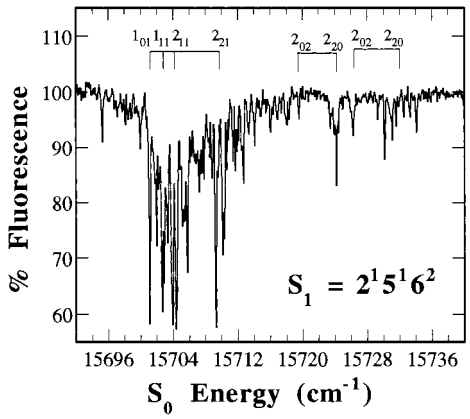

Figure 3. $S_1 = 2^15^16^2$ SEP spectrum in the vicinity of the DF peak near 15 700 cm^{-1} shown in Figure 1. The spectrum was recorded with perpendicular polarization at low resolution. A strong A″ band appears with its origin at 15 700.3 cm^{-1}, and two weaker A′ bands appear at 15 715.8 and 15 724.1 cm^{-1} (The 0_{00} lines appear in the parallel polarization scan only). Clumps consist of vibrational eigenstates with common $J_{K_aK_c}$ rotational assignments (as indicated for each band).

comprise a group. Groups form progressions in the CO stretching frequency, ν_2 (1804.23 cm^{-1} [21]). This is in accord with Franck−Condon arguments based on the significant difference in the length of the CO bond in S_0 (1.181 Å) and S_1 (1.3442 Å).[32] The Franck−Condon intensity is more evenly distributed in the 5^16^6 spectrum, though progressions in ν_2 are still discernible. The dissimilarities in these two spectra may result from differences in the zero-order Franck−Condon factors for transitions from these two S_1 states or from differences in the coupling between the Franck−Condon active S_0 levels, in the two spectra, and the optically dark levels. These possibilities will be considered more fully in sections IV and V.

SEP spectra from the completely resolved 1_{10} lines of the 5^16^4 and $2^15^16^2$ vibrational levels of S_1 were recorded from 13 000 to 20 000 cm^{-1} on S_0. Additional SEP spectra were recorded from 15 500 to 15 900 cm^{-1} on S_0 from the 1_{10} lines of the 6^6, 2^2, 5^26^4, 5^16^6, and 2^16^4 vibrational levels of S_1 (Figure 2). For measuring dissociation rates of SEP-prepared states via a pump−dump−probe scheme, it is advantageous to pump an S_1 level with a short fluorescence lifetime. Therefore, as preliminary experiments for rate measurements, SEP spectra were also recorded from 15 650 to 16 690 cm^{-1} from the short-lived ($\tau = 58$ ns) $2^13^16^2$ vibrational level of S_1. Vibrational band energies and symmetries, obtained from these spectra, are listed in Tables 2 and 3. The energy of the 0_{00} level is listed for A′ bands. For A″ bands, the 0_{00} line is not observed and the energy of the 1_{01} level is listed. This level is approximately 0.7 cm^{-1} above the vibrational origin. When a Franck−Condon-allowed line is split into a multiplet, the energy of the most intense line is given. The dumping efficiency of the strongest line in each band is also listed. Relative dumping efficiencies are only accurate in small-energy regions (approximately 300 cm^{-1}) due to variations in the dump power over the gain curve of a laser dye and from dye to dye. Over large regions, dumping efficiencies are only accurate to within a factor of 3.

Vibrational states containing an even (odd) number of quanta in ν_6 have A′ (A″) vibrational symmetry. Vibrational symmetry assignments of SEP spectra were made by examining the polarization dependence of the rotational fine structure, as described previously.[21] SEP spectra reveal that the majority of the DF peaks are composed of multiple vibrational bands (Figures 3 and 4). Thus, following the terminology of Yamanouchi et al., DF peaks are called features.[33] In many cases, vibrational bands having both A′ and A″ symmetry are observed under a single DF feature (Figure 3). However, the strongest transitions under the DF features comprising a given group in the $2^15^16^2$ DF spectrum have a common symmetry. For example, the most intense transitions in the group of features near 15 800 cm^{-1} in the $2^15^16^2$ DF spectrum are A″ vibrational states (Figures 3 and 4). The strongest lines in adjacent groups of features have opposite symmetries, and groups with A″ symmetry (e.g., 14 000, 15 800 cm^{-1}) are more intense than A′ groups (e.g., 13 200, 15 000 cm^{-1}) (Figure 1).

Closer inspection of the spectra in Figures 3 and 4 reveals that many of the SEP bands are comprised of clumps of vibrational eigenstates. For example, the clumps of lines labeled 1_{01} and 1_{11} in the intense A″ band in Figure 4 disappear completely in the parallel polarization scan, indicating that these states are all $J = 1$ levels. As discussed below, there is no evidence for Coriolis coupling of the 1_{01} levels to the back-

TABLE 2: Vibrational Energies and Dumping Efficiencies[a]

obsd (cm^{-1})	sym	dumping efficiency (%) S_1 vibrational state 5^16^4	$2^15^16^2$	$2^13^16^2$	obsd (cm^{-1})	sym[b]	dumping efficiency (%) S_1 vibrational state 5^16^4	$2^15^16^2$	$2^13^16^2$	obsd (cm^{-1})	sym[b]	dumping efficiency (%) S_1 vibrational state 5^16^4	$2^15^16^2$	$2^13^16^2$
13 270.0	A″	21			15 379.0	A′		20		17 023.7	?		9	
13 365.9	A″	26			15 396.5	A″		10		17 053.8	up		68	
13 490.5	A′	40			15 403.1	A″		26		17 070.2	A″		28	
13 507.9	A″	15			15 415.3	A′		13		17 078.0	?	9		
13 540.4	A″	18	6		15 462.1	?	19			17 088.5	A″		15	
13 650.2	?	21			15 465.8	A″		17		17 111.6	?	46		
13 683.7	A′	21			15 467.5	?		22		17 123.1	up		24	
13 775.4	A′	50	10		15 918.9	up		22		17 186.2	?		49	
13 808.0	?		11		15 934.8	?		7		17 243.2	up		48	
13 849.5	A′	39	16		15 986.9	A″		14		17 278.0	A″	33		
13 859.4	A′		10		16 010.0	A′		15	17	17 279.7	?		36	
13 889.7	?		13		16 015.4	A″		14	18	17 297.0	?	37		
13 900.4	A″	40			16 031.0	?			8	17 325.9	up		34	
13 923.9	A′		23		16 026.5	?		11		17 364.0	?	32		
13 929.5	A″	17			16 037.8	A″		8		17 383.1	?		48	
13 973.0	A′	10	26		16 085.1	A′	12			17 454.4	A′		19	
13 999.3	A″	17			16 087.9	?			11	17 459.2	A″		70	
14 012.1	A″	16	50		16 097.9	A′		41	17	17 482.0	?	19		
14 028.8	A′		18		16 122.6	?		13		17 482.5	A′		21	
14 050.5	A″		10		16 131.3	A″		10		17 485.1	A″		78	
14 099.7	?		30		16 194.2	A′		8	21	17 500.0	?	11		
14 112.2	A″	50	40		16 207.0	A′		12		17 516.3	up		19	
14 119.6	A′	20	26		16 217.0	?			12	17 610.0	up		41	
14 134.0	A″		9		16 230.2	?			12	17 640.0	up		12	
14 229.8	A′		6		16 230.6	?		5		17 698.0	up		27	
14 242.0	A″		10		16 233.0	?	11			17 747.5	up	70		
14 281.7	A′		4		16 242.8	?		5		17 764.3	up	80		
14 283.2	A′	15			16 297.0	?			9	17 790.0	A″		24	
14 298.7	A′	14			16 325.2	A″		17		17 794.6	A′		18	
14 314.7	A′	5			16 325.4	A″			19	17 894.5	up		36	
14 337.3	A″	24			16 333.5	A′			24	17 908.8	A′		13	
14 394.0	A′		11		16 351.3	A′		14	26	17 954.1	up	98		
14 401.3	A′	21			16 348.0	?	38			17 992.4	?		9	
14 405.4	A′	10			16 377.1	A′		10		18 013.0	?	15		
14 430.0	?	7			16 386.1	A″		17		18 060.6	?		14	
14 533.0	A″	12			16 386.8	A″			9	18 085.8	A″	5		
14 568.0	?	21			16 414.2	up		56		18 116.0	?	12	19	
14 658.5	A″	4			16 427.8	?		20		18 149.0	?		14	
14 673.0	A″	35			16 427.8	A″			18	18 174.0	?	11		
14 684.8	A′	6	19		16 443.4	?		22		18 218.8	up	100		
14 706.6	A′	7			16 442.3	A′			8	18 257.3	up		63	
14 707.9	A″		9		16 448.0	?	29			18 300.0	?		19	
14 721.8	A′	6			16 463.1	A″		24		18 332.6	A′	11	25	
14 727.8	A′	7	4		16 474.5	A′		20		18 413.7	up	92		
14 752.2	A′	23	26		16 487.3	A′		24		18 428.1	up	100		
14 763.0	?	10			16 540.2	A″		12		18 441.8	A′	12	10	
14 769.8	A″		19		16 551.6	A′		24		18 465.6	?		9	
14 792.9	A′		29		16 562.2	A″	14			18 543.0	?	14		
14 808.2	A′	15	46		16 557.4	A″		41		18 546.4	up		94	
14 832.5	A″		7		16 606.1	A′	21			18 571.0	up		23	
14 873.0	A″		19		16 611.0	A′		32		18 629.7	up	90		
14 874.0	A′		32		16 612.6	A″		44		18 637.2	A″	10		
14 886.0	A′		39		16 618.2	A″		35		18 730.0	?		44	
14 904.0	A′		10		16 623.1	A′	20			18 770.6	up		60	
14 930.4	A′		10		16 647.5	A′		63		18 886.5	up	86		
14 950.1	A″		29		16 652.4	A′	12			18 936.0	up		53	
14 963.7	A′	17	50		16 708.5	?	14	21		18 958.3	up		29	
14 968.6	A″	16	17		16 759.0	?	10			19 001.6	up		23	
14 984.3	A′		14		16 744.3	A″		32		19 049.9	A′	10	10	
15 034.8	A′		17		16 761.1	A′		48		19 065.5	A′	5	14	
15 055.8	A″		4		16 761.8	A″		50		19 100.6	up	100		
15 101.6	A′		5		16 772.0	A′		16		19 148.0	?		16	
15 168.2	A″		9		16 810.3	?	19			19 196.6	up		66	
15 179.7	A′		13		16 833.1	A′		32		19 215.0	up		34	
15 246.4	A″		19		16 866.4	?		27		19 260.8	?	9		
15 255.0	?	6			16 914.9	?	18			19 275.4	?		13	
15 266.0	?	11	8		16 915.8	A′		18		19 304.5	?	11		
15 285.8	A′		14		16 947.0	A″		50		19 393.3	up		30	
15 354.4	A′		10		16 974.2	A′		50		19 418.3	up		11	
15 358.2	A″		15		16 975.6	?	6			19 783.2	?	15		

[a] For 15500−15900 cm^{-1}, see Table 3. [b] Up designates upward transitions.

TABLE 3: SEP Spectrum of the $N = 9.5$ Polyad

obsd (cm^{-1})	sym	dumping efficiency (%) S_1 vibrational state pumped $5^1 6^4$	6^6	2^2	$2^1 5^1 6^2$	$5^2 6^4$	$5^1 6^6$	$2^1 6^4$	$2^1 3^1 6^2$
15 499.8	?			19					
15 500.3	A″		31		28		32	17	
15 502.8	A″		49		27	11	20	17	
15 510.8	A′		10						
15 518.0	?						16		
15 518.5	A″					7			
15 518.9	A′	37				8			
15 520.4	?				8				
15 540.2	A′				18				
15 543.4	A″			12					
15 554.0	?						16		
15 559.8	A′	8			23				
15 577.9	A″	11			19	8			
15 592.3	A″				21				
15 592.9	A″						17	45	
15 595.1	A′	14							
15 595.2	A″	49			36	42			
15 603.0	A′	9							
15 603.2	A′			14					
15 610.3	A′				17				
15 612.0	?					16			
15 618.9	?	19							
15 620.4	?					21			
15 631.1	up	27							
15 636.4	?			11					
15 642.9	A″		7				13	15	
15 658.8	A′	13	6		38				
15 692.1	A′	6	6				21		
15 692.7	A′			25					
15 694.1	?						28		
15 700.3	A″	16	28		43	31	20	38	
15 715.2	A′					8			
15 715.7	?			43					
15 715.8	A′		21		36		15		
15 720.0	A″							22	
15 720.9	A″					11			

obsd (cm^{-1})	sym	dumping efficiency (%) S_1 vibrational state pumped $5^1 6^4$	6^6	2^2	$2^1 5^1 6^2$	$5^2 6^4$	$5^1 6^6$	$2^1 6^4$	$2^1 3^1 6^2$
15 723.6	A′	11							
15 724.1	A′		8		14		27		
15 751.1	A″	4						12	
15 760.0	A″				16				
15 764.4	?			15					
15 769.0	A′				16				
15 778.2	A″	3							
15 784.5	A″				7				
15 785.4	A″		8						
15 790.7	A″					32			
15 798.2	A′				15				
15 798.6	?			17					
15 803.6	A″	43			50	42			14
15 805.1	?		5					12	
15 812.0	A′	6			14				
15 815.0	A″	16							
15 823.0	?		3						
15 825.7	?			15					
15 826.7	A″						35		
15 827.3	?							50	
15 827.7	A″				12				
15 828.4	?		19						
15 832.5	A″	27			20				
15 844.6	A″	4					13		
15 852.9	A′						15		
15 861.0	?							6	
15 863.2	A′				11				
15 863.6	?					11			
15 870.1	A″					23			
15 870.7	?			23					
15 873.3	?	8							
15 878.1	?		3						
15 881.0	A′						7		
15 885.1	A″				13				
15 889.8	?			8					

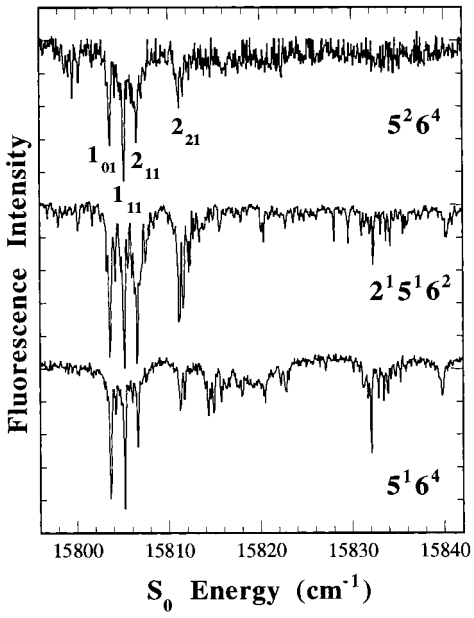

Figure 4. SEP spectra from three S_1 vibrational states in the vicinity of the DF peak near 15 800 cm^{-1} shown in Figure 1. Spectra were recorded with perpendicular polarization at low resolution. In all three spectra the baseline is at 100% fluorescence and ticks indicate increments of 10% in dumping efficiency. An intense A″ band appears in all three spectra at 15 803.6 cm^{-1}.

ground levels. A-type Coriolis coupling of 1_{11} levels is weak and does not result in an increased number of resolvable lines. Thus, the vibrational eigenstates comprising clumps in these figures all have the same rotational wave function.

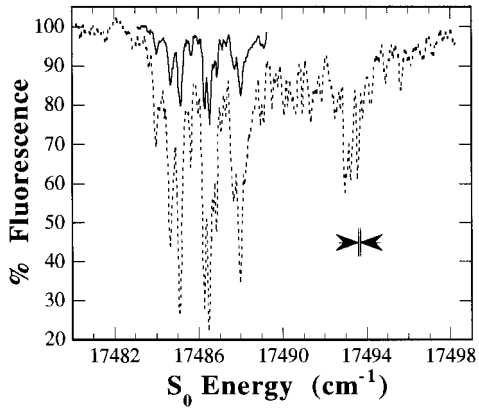

Figure 5. $S_1 = 2^1 5^1 6^2$ SEP spectra. Dumping efficiencies greater than 50% (- - -) indicate significant dissociation on the time scale of the 10 ns laser pulse. The same spectrum was recorded with reduced dump laser power (−) to eliminate saturation broadening effects. The spectral line widths are larger than the laser bandwidth indicated in the figure with arrows.

Dumping efficiencies of greater than 50% were observed for several strong transitions. The strongest transitions in the SEP spectrum are under the features near 15 800 and 17 500 cm^{-1}. The intense A″ band in Figure 4 saturates at 50% dumping efficiency, but a dumping efficiency of 78% is achieved for the intense band in Figure 5. This is possible only if the S_0 level is dissociating on the time scale of the 10 ns laser pulse. The weaker spectrum in Figure 5 was recorded with reduced laser power to distinguish between saturation and lifetime broadening. At reduced power, the line widths are still broader than the laser bandwidth by more than a factor of 2 and no

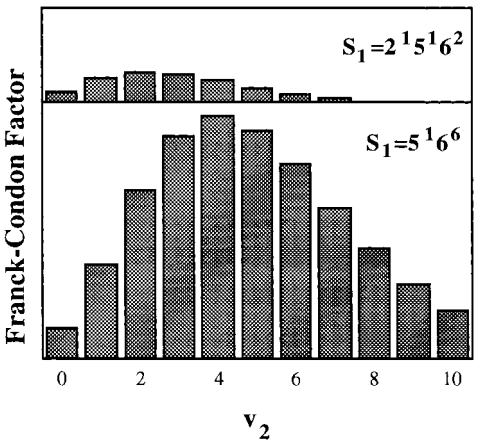

Figure 6. Calculated zero-order Franck−Condon factors for the ν_2 progression originating from the $2^1 5^1 6^2$ and $5^1 6^6$ vibrational levels of S_1. The values of all other S_0 vibrational quantum numbers are held fixed at 0. The scale is the same in the top and bottom. The $2^1 5^1 6^2$ Franck−Condon factors are smaller than the $5^1 6^6$ Franck−Condon factors for states with $\upsilon_6 = 0$ (see Figure 7).

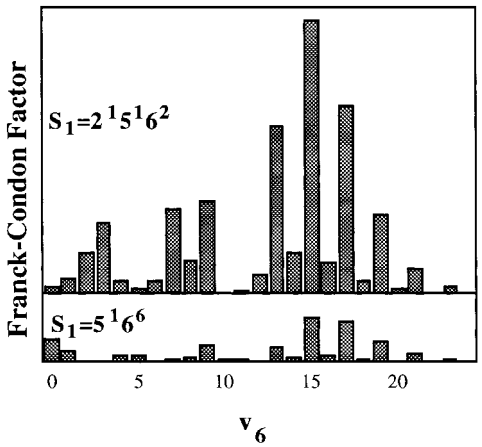

Figure 7. Calculated zero-order Franck−Condon factors for the ν_6 progression originating from the $2^1 5^1 6^2$ and $5^1 6^6$ vibrational levels of S_1. The values of all other S_0 vibrational quantum numbers are held fixed at 0. The scale is the same in the top and bottom.

additional structure appears. Line width broadening, $\Delta\nu$ (fwhm), is related to the unimolecular dissociation rate, k_d, by[34]

$$k_d = 2\pi c\Delta\nu \tag{1}$$

Measured dissociation rates of DFCO near 16 000 cm^{-1} are between 1×10^7 and 1×10^8 s^{-1}, implying a dissociation barrier between 17 000 and 17 300 cm^{-1}.[35] The calculated RRKM dissociation rate at 17 500 cm^{-1}, assuming a barrier of 17 000 cm^{-1}, is 5×10^9 s^{-1}, corresponding to a line width of only 0.03 cm^{-1}. However, the RRKM rate assuming a barrier of 16 500 cm^{-1} results in a line width of 0.07 cm^{-1}. Given, the ±1400 cm^{-1} uncertainty in the barrier height and the questionable applicability of RRKM theory to formyl fluoride,[10] lifetime broadening cannot be ruled out at 17 500 cm^{-1}.

Upward transitions to higher lying electronic states are also identified in the SEP spectrum. At longer dumping wavelengths (lower total energy, $E_{tot} = E_{pump} + E_{dump}$), upward transitions appear more frequently. These are often sharp intense lines in the spectrum that do not correlate with dispersed fluorescence intensity. Upward transitions are observed at total energies as low as 58 489 cm^{-1}. A broad structureless transition, showing no polarization dependence, appears in the $5^1 6^4$ spectrum near 15 631 cm^{-1} (Figure 2). A similar band is observed at the same total energy (63 146 cm^{-1}) in the $2^1 5^1 6^2$ SEP spectrum at 16 414 cm^{-1}, suggesting that this is an upward transition.

IV. Vibrational Assignment of Franck−Condon Active States

Due to the large changes in the equilibrium values of the CO bond length and the out-of-plane angle between S_0 and S_1, ν_2 and ν_6 are predicted to be the most strongly Franck−Condon active modes of formyl fluoride. This is supported by both experimental results and calculations.[16,21,29] Forty-eight vibrational bands in the 6^4 SEP spectrum of HFCO were assigned to 2_n6_m progressions with values of n ranging from 0 to 5 and values of m ranging from 6 to 23.[16] The DFCO SEP spectrum below 9000 cm^{-1} was also assigned primarily in terms of progressions in ν_2 and ν_6.[21]

Franck−Condon factors for ν_2 and ν_6 progressions originating from the $2^1 5^1 6^2$ and $5^1 6^6$ vibrational levels of S_1 were calculated as described in ref 28. The results are shown in Figures 6 and 7. ν_2 progressions originating from $2^1 5^1 6^2$ and $5^1 6^6$ peak at $\upsilon_2 = 2$ and 4, respectively. The pure ν_2 Franck−Condon factors from $5^1 6^6$ are up to a factor of 8 larger than those from $2^1 5^1 6^2$. The ν_6 progressions from these two S_1 levels are significantly different. The $2^1 5^1 6^2$ ν_6 progression peaks strongly at $\upsilon_6 = 15$, with smaller peaks at $\upsilon_6 = 9$ and 3. The $5^1 6^6$ υ_6 progression is more diffuse, with several weak peaks at $\upsilon_6 = 0$, 9, and 15. These differences can be understood by examining the S_1 6^2 and 6^6 double-well wave functions (see Figure 7, ref 21). In the lower energy 6^2 state, the probability density is largest near the minima along the out-of-plane coordinate. These minima correspond to large values of the out-of-plane bending angle and overlap most strongly with highly vibrationally excited S_0 ν_6 wave functions. The probability density of the higher energy $S_1 = 6^6$ vibration has a maximum at the planar configuration, and, therefore overlaps more strongly with the S_0 $\upsilon_6 = 0$ wave function.

The energies of the zero-order 2_n6_m progressions for $n = 0-4$ and $m = 13-19$ are labeled in Figure 1. Also shown are the zero-order energies of the 2_n6_8, 2_n6_{10}, and 2_n6_{12} progressions for $n = 2-7$, $n = 1-6$, and $n = 0-5$, respectively. These energies are calculated from the Dunham expression using the experimentally determined spectroscopic constants listed in ref 21 (Table 3, column 2).

$$E(\upsilon_1\upsilon_2\upsilon_3\upsilon_4\upsilon_5\upsilon_6) = \sum_i \omega_i\upsilon_i + \sum_{i,j\geq i} x_{ij}\upsilon_i\upsilon_j \tag{2}$$

In this expression, the ω_i's and the x_{ij}'s are the harmonic frequencies and anharmonic constants and the υ_i's are vibrational quantum numbers. The groups of intense features in the $2^1 5^1 6^2$ DF spectrum correlate closely with the energies of the calculated 2_n6_m ($n = 0-4$, $m = 13-19$) progressions shown in Figure 1. As discussed above, these zero-order progressions have the largest calculated Franck−Condon factors. States with similar amounts of excitation in ν_6 are Franck−Condon active in the HFCO 6^4 spectrum,[16] supporting the assignment of these states as the Franck−Condon active zero-order states in the DFCO $2^1 5^1 6^2$ spectrum. These similarities result from similarities between the HFCO and DFCO S_1 ν_6 wave functions. The $5^1 6^6$ DF spectrum is more congested, however, progressions in ν_2 can be identified and correlate closely with the calculated zero-order energies of 2_n6_m ($n = 2-6$, $m = 8-12$) states. These are the zero-order states predicted to have the largest Franck−Condon factors from $S_1 = 5^1 6^6$. The more uniform $5^1 6^6$ Franck−Condon envelope is also predicted by the calculation shown in Figure 7.

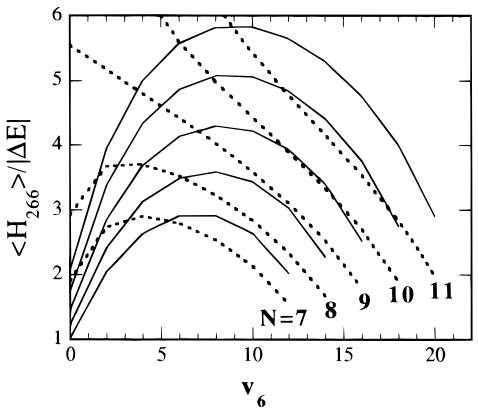

Figure 8. Coupling strength, $\langle H_{266}\rangle/|\Delta E|$, between the zero-order states 2_n6_m and $2_{n-1}6_{m+2}$. This is plotted as a function of the ν_6 quantum number for the $N = \upsilon_2 + \upsilon_6/2$ polyads with $N = 7-11$. Data are calculated using the spectroscopic constants given in columns 1 (···) and 2 (—) of Table 3 in ref 21.

The Franck−Condon factor calculations predict the type of qualitative differences between 5^16^6 and $2^15^16^2$ spectra that are observed. However, the agreement between the calculated zero-order and the experimental spectra does not yield conclusive assignments. First, short progressions in ν_5 were observed in the DFCO spectrum below 9000 cm^{-1},[21] and Franck−Condon calculations indicate that states with 2−4 quanta in ν_5 are weakly Franck−Condon active. This may account for additional features in the spectra. More important is the strong 266 ($\nu_2 \approx 2\nu_6$) Fermi resonance that was identified in analysis of the low-energy DFCO spectrum.[21] This resonance defines polyads of approximately isoenergetic-coupled zero-order vibrational states. For example, the states 2_2, 2_16_2, and 6_4 constitute a 266 polyad. Thus, the zero-order states predicted to carry the oscillator strength in these SEP experiments are directly coupled by Fermi resonance. The 266 Fermi resonance destroys the zero-order ν_2 and ν_6 quantum numbers but conserves the value of the polyad number N defined as

$$N = \upsilon_2 + \upsilon_6/2 \tag{3}$$

The coupling matrix element, $\langle H_{266}\rangle$, representing the 266 Fermi interaction between the states 2_n6_m and $2_{n-1}6_{m+2}$ is given, in a harmonic oscillator basis, by[36,37]

$$\langle H_{266}\rangle = \langle \upsilon_2 - 1, \upsilon_6 + 2|k_{266}Q_2Q_6Q_6|\upsilon_2, \upsilon_6\rangle = (k_{266}/2\sqrt{2})[\upsilon_2(\upsilon_6+1)(\upsilon_6+2)]^{1/2} \tag{4}$$

Here k_{266} is the coefficient of the $Q_2Q_6Q_6$ term in the expansion of the potential-energy function in normal coordinates. The value of k_{266} is determined experimentally to be between 42 and 44 cm^{-1}.[21] The coupling of the zero-order vibrational states within the polyads can cause significant shifts from the zero-order energies. Similarly, since the eigenstates of the polyad can be strongly mixed combinations of the zero-order states, the observed spectral intensity may differ significantly from the zero-order Franck−Condon factors. The strength of the resonance is determined by the ratio $\langle H_{266}\rangle/\Delta E$, where ΔE is the energy separation between two coupled zero-order states in the polyad calculated using eq 2.

The two sets of experimentally determined constants[21] were used to predict the strength of the 266 resonance as a function of the v_6 quantum number within a polyad and as a function of the polyad number N (Figure 8). For a given polyad N, both sets of constants predict that the coupling strength is weaker for the zero-order states 6_{2N} than for the states near the middle of the polyad. The predicted coupling strength either increases or decreases toward the 2_N side of the polyad depending on which set of constants is used. However, since the states 2_N are not predicted to be FC active, this difference does not affect the present analysis. These results also indicate that the coupling strength increases for higher polyads. Comparison of Figures 7 and 8 suggests that, compared to the $2^15^16^2$ spectrum, the Franck−Condon active states in the 5^16^6 spectrum are more strongly coupled members of the 266 polyads.

Due to the strong anharmonic mixing caused by the 266 resonance, the zero-order vibrational assignments (Figure 1) are more appropriately replaced by polyad number assignments (also shown in Figure 1). For example, in the $2^15^16^2$ spectrum, the strong A″ states near 14 000 (near 6_{17}, 2_16_{15}, 2_26_{13} in Figure 1) and 15 800 cm^{-1} (near 2_16_{17}, 2_26_{15}, 2_36_{13} in Figure 1) are members of the $N = 8.5$ and 9.5 polyads, respectively. The weaker A′ states under these same DF features are members of the $N = 8$ and 9 polyads, respectively. The evidence for vibrational coupling and polyads is explored more fully in the next section.

V. Vibrational Coupling and IVR in the SEP Spectrum

It is of interest, for understanding the DFCO IVR rates and mechanisms, to determine if spectral lines derive their intensity from a common Franck−Condon active vibrational state or from independently Franck−Condon active vibrational states. The fastest IVR rates result from the strongest vibrational couplings and are characterized by the distribution of a single zero-order Franck−Condon factor over the broadest energy range. Slower IVR processes, resulting from smaller coupling matrix elements, are evident in the spectrum at higher resolution. If the intensity in a portion of the spectrum results from the distribution of a single zero-order Franck−Condon factor, then the coupled vibrational states will always appear as a set with the same relative intensities in SEP spectra from different S_1 levels. However, if there is more than one Franck−Condon active zero-order state and those states are coupled, interferences may alter the relative intensities of these states in spectra recorded from different S_1 levels. In extreme cases, strong interferences can potentially result in the complete disappearance of some members of the polyad. As discussed, previous results suggest that a strong 266 resonance couples zero-order vibrational states into polyads. Additionally, other weaker resonances, identified in the spectrum below 9000 cm^{-1}, may further couple the Franck−Condon active states with background states on a slower time scale.[21] This, in combination with the calculations in the previous section suggest that the groups of features in the $2^15^16^2$ DF spectrum are polyads of coupled zero-order 2_n6_m vibrational states. To test this, SEP spectra were recorded in the region of the $2^15^16^2$ DF features near 15 800 cm^{-1} from several different S_1 vibrational levels. Spectra are compared from the view that coupled states always appear as an indivisible set (in the absence of interferences). Figure 2 shows the spectra from 15 500 to 15 900 cm^{-1} on S_0, recorded from the 1_{10} levels of the 5^16^4, 6^6, 2^2, $2^15^16^2$, 5^26^4, 5^16^6, and 2^16^4 vibrational states of S_1.

SEP spectra under adjacent DF peaks are compared to determine whether large coupling matrix elements exist which are responsible for rapid IVR. As noted, the strongest transitions under the features near 15 800 cm^{-1} in the $2^15^16^2$ DF spectrum (Figure 2) are the A″ vibrations at 15 595.2, 15 700.3, and 15 803.6 cm^{-1}. The strong bands with origins at 15 700.3 (Figure 3) and 15803.6 cm^{-1} (Figure 4) appear in the 5^16^4,

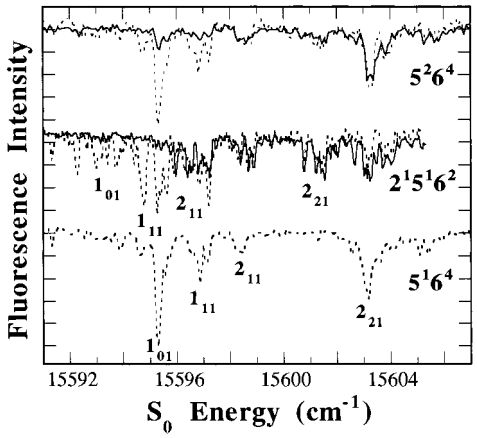

Figure 9. SEP spectra in the vicinity of the DF feature near 15 600 cm^{-1}. Spectra recorded with perpendicular (···) and parallel (—) polarization are overlaid in the $2^15^16^2$ and 5^26^4 spectra. In all three spectra the baseline is at 100% fluorescence and ticks indicate increments of 10% in dumping efficiency.

$2^15^16^2$, and 5^26^4 SEP spectra. The band at 15 595.2 cm^{-1} dominates the 5^16^4 spectrum and appears in all three spectra (Figure 9), although the $2^15^16^2$ spectrum is significantly more complicated. The 5^16^4 and 5^26^4 spectra have a typical A″ rotational structure that exhibits the expected polarization dependence. Polarization experiments in the $2^15^16^2$ spectrum indicate that the lines appearing on the low-frequency side of the main band between 15 592 and 15 596 cm^{-1} in the perpendicular scan are the $J = 1$ lines from a second clump of A″ vibrational states centered near 15 593 cm^{-1}. This second clump appears to gain intensity from a separate Franck−Condon factor since none of these lines appear in the other spectra. A fourth weaker A″ band also appears in these three spectra at 15 577.9 cm^{-1}. The three A″ bands at 15 577.9, 15 595.2, and 15 803.6 cm^{-1} appear as a set in all three spectra, and none of these bands appear independently in SEP spectra from other S_1 levels. This implies that these states are members of the $N = 9.5$ 266 polyad that derive their transition strength from a common zero-order Franck−Condon active state. Moreover, the values of the 266 coupling matrix elements in this polyad are approximately 200 cm^{-1}, resulting in an eigenvalue spacing equal to the separation between the DF peaks near 15 600 and 15 800 cm^{-1}. The presence of a second coupled level (15 577.9 cm^{-1}), under the DF feature near 15 600 cm^{-1}, reflects an additional coupling mechanism and is discussed below. The strong band in Figure 3 at 15 700.3 cm^{-1} does appear in SEP spectra from other S_1 levels, and its intensity may result from a separate set of Franck−Condon factors.

The relative intensities of the bands at 15 577.9, 15 595.2, and 15 803.6 cm^{-1} in these three SEP spectra are 1:5:4 (5^16^4), 1:2:3 ($2^15^16^2$), and 1:5:5 (5^26^4). The $2^15^16^2$ ratio differs slightly from the relative intensity of the corresponding DF features for several reasons. First, although these are the strongest transitions under the DF peaks, additional bands contribute to the fluorescence intensity. Second, relative SEP intensities are not accurate over long wavelength scans due to variations in the dump power over the gain curve of the dye. Third, saturation of the band at 15 803.6 cm^{-1} in the $2^15^16^2$ spectrum results in a smaller observed intensity ratio for the bands at 15 595.2 and 15 803.6 cm^{-1}. The variation of the relative intensities in the three spectra nevertheless supports the notion that there is more than one Franck−Condon active state per polyad.

The distribution of Franck−Condon intensity among the eigenstates comprising a group of features in the $2^15^16^2$ DF

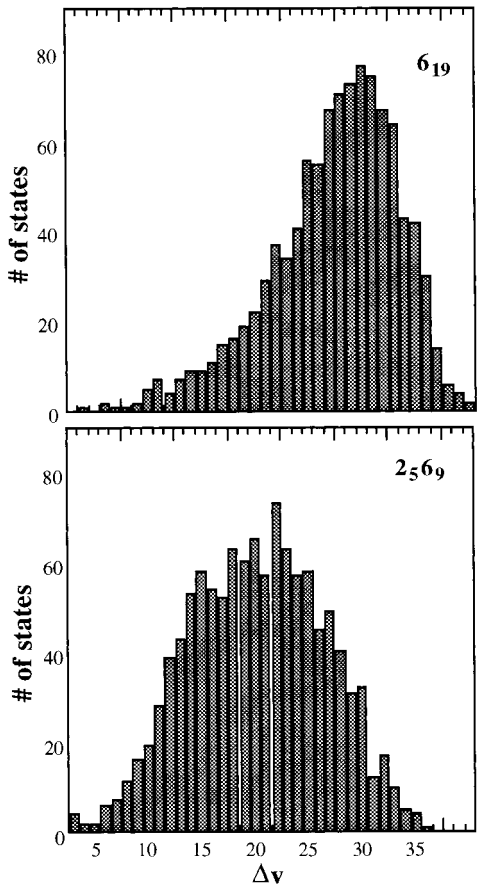

Figure 10. Histograms of the quantum-number changes between the zero-order states 6_{19} and 2_56_9 and the bath states. 6_{19} is far away in vibrational quantum-number space from most isoenergetic bath states. The average (over all modes of all bath states) vibrational quantum number for a mode of the bath is 3.

spectrum, implies values for the IVR coupling matrix elements that are on the order of the 200 cm^{-1} group width and translates to an IVR time of 25 fs. The 266 resonance, proposed to account for this rapid coupling, causes vibrational energy transfer from the out-of-plane bend to the CO stretching vibration. For example, the Franck−Condon active state 6_{19} rapidly couples to the states 2_16_{17}, 2_26_{15}, and so on via sequential $\Delta v = 3$ transitions. Thus, zero-order, extreme-motion, out-of-plane bending vibrations that exhibit stability against IVR in HFCO are not observed in DFCO. The 266 resonance removes the bottleneck to IVR out of ν_6 in DFCO, and this rapid initial mixing facilitates further coupling to the background states. These dynamical differences between HFCO and DFCO indicate the relative importance of low-order ($\Delta v = 3,4$) and high-order ($\Delta v \geq 5$) resonances at these energies and state densities. Since the magnitude of the coupling matrix elements decreases with increasing Δv,[13] low-order resonances are often implicated in the fastest time scales of IVR.

Figure 10 shows histograms of the quantum-number changes between zero-order states in the $N = 9.5$ polyad and the zero-order background states in an energy window of ±100 cm^{-1}. The number of states that are potentially coupled to the 2_56_9 state via low-order resonances is significantly larger than for the 6_{19} state. Thus, the 266 resonance brings the extreme-motion, Franck−Condon active, zero-order states closer in quantum-number space to the bath of background states. Weaker 233 ($\nu_2 \approx 2\nu_3$, $k_{233} = 23-27$ cm^{-1}) and 3566 ($2\nu_6 \approx \nu_3 + \nu_5$, $k_{3566} = 5-11$ cm^{-1}) resonances were also identified in the analysis of the DFCO spectrum below 9000 cm^{-1} [21] and

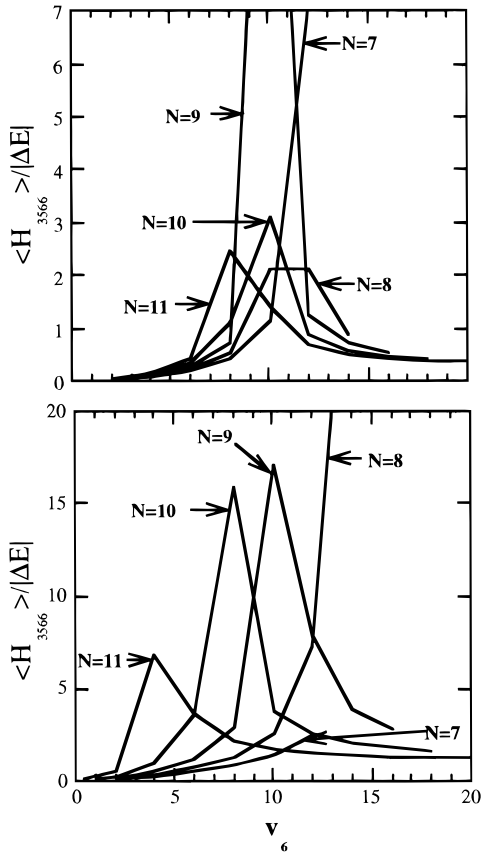

Figure 11. Coupling strength, $\langle H_{3566}\rangle/|\Delta E|$, between the zero-order states 2_n6_m and $2_n3_15_16_{m-2}$. Coupling strength is plotted as a function of the υ_6 quantum number for the $N = \upsilon_2 + \upsilon_6/2$ polyads with $N = 7-11$. Data are calculated using the spectroscopic constants given in columns 1 (top) and 2 (bottom) of Table 3 in ref 21.

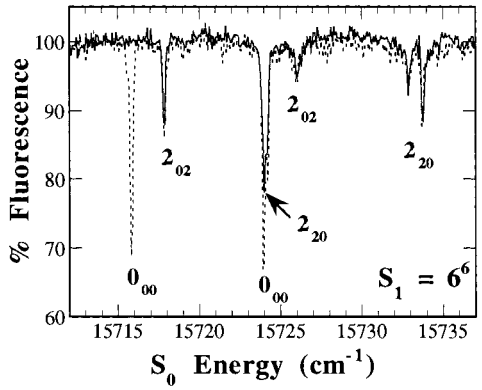

Figure 12. SEP spectra from the 6^6 vibrational level of S_1. Spectra recorded with parallel (···) and perpendicular (—) relative polarization are overlaid. Rotational assignments ($J_{K_aK_c}$) are indicated. Two anharmonically coupled A′ vibrational bands are observed. The increased line width and splitting of the 2_{20} rotational levels, compared to the $K_a = 0$ levels, suggests A-type Coriolis coupling to an A″ vibrational level.

may result in further coupling of the 2_n6_m states to background states with excitation in ν_3 and ν_5. Figure 11 shows the strength of the 3566 resonance, calculated from the data in Table 4 of ref 21, as a function of υ_6 for polyads $N = 7-11$. Both sets of constants predict that this resonance is strong for states in these polyads with values of υ_6 between 4 and 15. These additional resonances result in expanded polyads. Since the coupling constants are smaller than those for the 266 resonance, these interactions result in IVR on a slower time scale. Due to high state densities, the large number of interacting levels, and multiple interfering Franck−Condon active states, exact spectroscopic deperturbation and assignment are not feasible. Dynamics on the next slower time scale are reflected by the spectral characteristics evident at the next higher level of resolution. To understand these processes, SEP spectra from different S_1 levels are compared in the vicinity of a single DF peak. As mentioned above, two coupled A″ peaks (15 577.9 and 15 595.2 cm^{-1}) appear under the DF feature near 15 600 cm^{-1}. Another weak A″ band (15 592.3 cm^{-1}) appears only in the $2^15^16^2$ spectrum (Figure 9). This band may disappear in the 5^16^4 and 5^26^4 spectra as a result of interferences. Similarly, five A″ bands appear under the $2^15^16^2$ DF feature near 15 800 cm^{-1}. Since four of these bands are weak, interferences may also cause these to disappear in the SEP from the other two S_1 levels. Interestingly, the calculated eigenstates near 15 600 and 15 800 cm^{-1}, in the 266 polyad, are split into a triplet and a quintet, respectively, by inclusion of the 233 and 3566 resonances. Additionally, the level spacings between these calculated states (10−30 cm^{-1}) are the same as those observed in the experimental spectrum. This suggests that the structure under individual DF peaks reflects the coupling via the 233 and 3566 resonances on a 500 fs time scale. Thus, the definition of the polyad is expanding with time. For example, by 500 fs, the 266 polyad number N is no longer conserved as vibrational energy couples from ν_2 and ν_6 into ν_3 (HCO bend) and ν_5 (FCO bend).

The spectrum in Figure 12 shows two A′ vibrational bands in the 6^6 spectrum. The lower energy band (15 715.8 cm^{-1}) is an A′ C-type band with rotational fine structure resembling that of vibrational states lying 10 000 cm^{-1} lower on the S_0 potential-energy surface.[21] A second A′ vibrational band is also observed at (15 724.1 cm^{-1}). Both states appear in the $S_1 = 6^6$, $2^15^16^2$, and 5^16^6 SEP spectra and neither appears independently in the other spectra, indicating that these states are anharmonically coupled. If only one state carries oscillator strength, the value of the anharmonic coupling matrix element, calculated from the relative intensities and energy separation of the 2_{02} levels, is 3.74 cm^{-1}. The zero-order states are separated by 3.55 cm^{-1}. Thus, vibrational energy oscillates between these two states with a period of 4 ps. The 2_{20} line of the lower frequency band is broadened, and the 2_{20} line of the higher frequency band is split into a doublet with a splitting of 0.87 cm^{-1}. The increased coupling of the bright and dark states with K_a is indicative of A-type Coriolis coupling. Additionally, the apparent rotational constant of the lower energy vibrational band is smaller (2.0 cm^{-1}) than that of the higher energy band (2.2 cm^{-1}). This also argues that in addition to the anharmonic coupling of the two A′ vibrations, there is a weaker A-type Coriolis-coupling mechanism.

The slowest IVR processes are reflected in the high-resolution spectrum. Several SEP spectra, in the vicinity of the $2^15^16^2$ DF line near 15 800 cm^{-1}, are shown in Figure 4. The strong A″ vibrational band at 15 803.6 cm^{-1} appears in the SEP spectra from these three S_1 levels. Another A″ vibrational band appears at 15 832.5 cm^{-1} in the $2^15^16^2$ and 5^16^4 spectra but is not observed in the 5^26^4 spectrum. Differences in the relative intensities of the rotational lines in the 15 803.6 cm^{-1} band in the three spectra result from partial saturation of the transitions in the $2^15^16^2$ and to a lesser degree the 5^16^4 spectra. Figure 13 shows a higher resolution ($\Delta\nu = 0.05$ cm^{-1}) close up of the $2^15^16^2$ spectrum recorded with reduced dump laser power. The intensities in this spectrum match those of the 5^26^4 spectrum more closely. The splitting of each rotational state in this band is reproduced, line for line, in all three spectra. This suggests that a single Franck−Condon active level is coupled to a

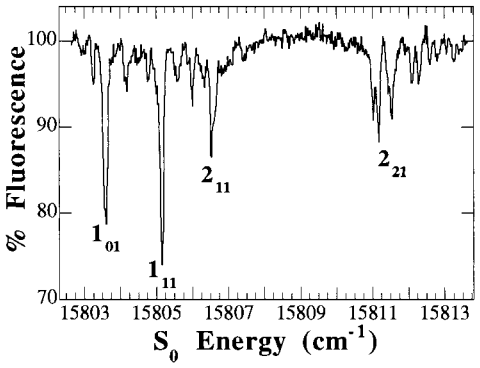

Figure 13. High-resolution (0.05 cm^{-1}) SEP scan from $S_1 = 2^1 5^1 6^2$. Observed line widths are larger than the laser bandwidth by as much as a factor of 4, implying unresolved vibrational structure.

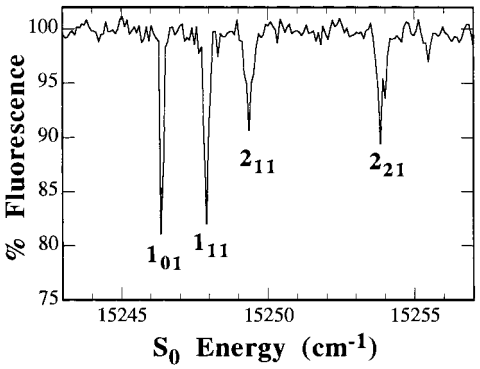

Figure 14. $S_1 = 2^1 5^1 6^2$ SEP spectrum of the A″ band at 15 246.4 cm^{-1}. The 1_{01} level appears stable against IVR. The increased line width ($K_a = 1$) and appearance of additional resolved lines ($K_a = 2$) compared to the 1_{01} line indicates weak A-type Coriolis coupling to background levels.

background of dark levels. The hybrid A/B-type rotational structure is still resolved, implying coupling matrix elements $\langle H \rangle$ that are smaller than the separation between the rotational lines ($\langle H \rangle \leq 1.5$ cm^{-1}). The fwhm of the three strongest lines in this band are 0.15 (1_{01}), 0.12 (1_{11}), and 0.19 cm^{-1} (2_{11}). These line widths are larger than the dump laser bandwidth. This is true even for the weakest transitions, where there is little chance of saturation broadening. Moreover, the fwhm of the 1_{11} line is narrower than that of the weaker 1_{01} line. The measured dissociation rates of states at this energy (approximately 1×10^7 to 1×10^8 s^{-1} [35]) are too slow to cause a lifetime broadening of 0.12 cm^{-1}. Thus, it is likely that there is unresolved vibrational structure under many of these SEP transitions. The coupling of nearby levels evident in these spectra indicate IVR between a Franck−Condon active state and a bath of background states on the time scale of approximately 4−44 ps (1.5−0.12 cm^{-1}).

A small number of lines show no evidence of weak anharmonic coupling. For example, the 1_{01} line of the A″ band in Figure 14 is laser bandwidth limited. As in the A′ bands shown in Figure 12, the line widths in this spectrum increase with K_a, indicating A-type Coriolis coupling. The 2_{11} line is twice the laser bandwidth, and the 2_{21} line is split into three resolvable states. The coupling matrix element inferred from the width and intensity distribution of the 2_{11} line is approximately 0.11 cm^{-1}, corresponding to a two-state oscillation period of 150 ps. Although there is no evidence of weak anharmonic coupling to the background levels, this state may be mixed with other A″ vibrational states in the 266 polyad.

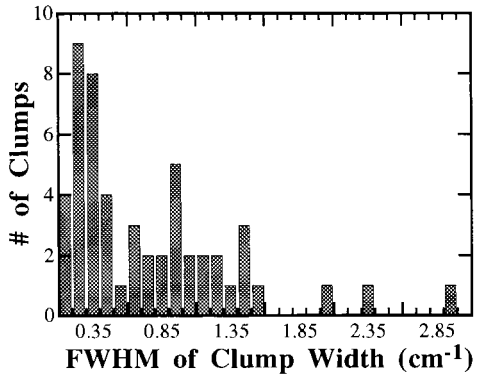

Figure 15. Distribution of clump widths (fwhm) for S_0 states (81% of symmetry assigned states) between 15 200 and 16 200 cm^{-1}.

VI. State Densities and IVR

Although several states show no evidence of weak anharmonic couplings (Figures 12 and 14), the majority (>99%) of the vibrational bands consist of clumps of vibrational eigenstates. Clump width is a measure of the IVR rate and varies from clump to clump. The distribution of clump widths for states with S_0 energies between 15 200 and 16 200 cm^{-1} is given in Figure 15. Clump widths are taken as the fwhm of the 0_{00} clumps (A′ bands) or 1_{01} clumps (A″ bands). For clump widths that are larger than the rotational-level spacing, the width is taken as twice the hwhm to the low-frequency half of the clump. Clump widths range from 0.11 to greater than 2 cm^{-1}, with a peak in the distribution between 0.25 and 0.35 cm^{-1}. The minimum observable width is given by the laser bandwidth (0.05 cm^{-1}). The range of observed widths corresponds to IVR times between 3 and 50 ps.

Comparison of the calculated and experimental state densities within these clumps measures the extent of IVR during the time period between 1 and 50 ps. State densities are calculated as the number of detectable lines, W, divided by the energy separation between the lowest and highest energy lines in the clump. The factor of $1/(W - 1)$ overestimate, introduced by this method, is typically less than 10%. As discussed above, most of the lines in the spectra are broader than the laser bandwidth. Below 17 000 cm^{-1}, the effects of saturation and lifetime broadening can be ruled out, suggesting unresolved vibrational structure. In many cases, this is supported by asymmetric line shapes. Thus, states are counted twice if the fwhm is greater than the laser bandwidth. A fwhm that is greater than twice the laser bandwidth is counted as three states. Due to unresolved structure, measured state densities represent a lower limit. At 10/cm^{-1}, equally spaced states with a Gaussian distribution of intensities are all resolvable at their fwhm. Weaker lines could remain undetected if occurring between two stronger lines or due to finite S/N. Increasing the density to 15/cm^{-1} results in a continuous intensity profile. At 8/cm^{-1}, equally spaced states are resolvable at 30% of their full intensity. At this density, only very weak peaks would remain undetected due to the finite S/N ratio or close proximity to a strong peak. State densities of A′ and A″ vibrational states are shown in Figure 16. Also shown are the calculated state densities (total and symmetry specific) based on an anharmonic direct count using eq 2 and the experimental spectroscopic constants listed in ref 21 (Table 3, column 2). The observed vibrational state densities approach the full calculated symmetry-specific vibrational state densities. Although there is some evidence for weak A-type Coriolis coupling, the state densities for $J = 2$, $K_a = 2$ states typically increase by no more than 25% over 0_{00} and 1_{01}

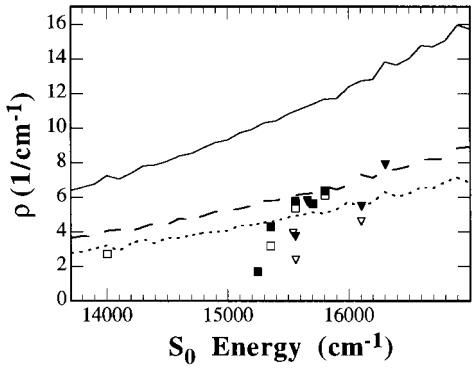

Figure 16. Vibrational density of states from an anharmonic direct count using experimentally determined values of spectroscopic constants. Total density (—), A′ density (- - -), and A″ (•••) density are shown. Also shown are experimental values for A′ (△) and A″ (□) states. Open symbols are for 0_{00} levels (A′ states) and 1_{01} levels (A″ states). Solid symbols are the values for states with $J = 2$ and $K_a = 2$.

states (filled symbols in Figure 16), much less than the factor of $(2J + 1)$ expected for complete K mixing. Thus, by 50 ps (approximately 10^3-10^4 times faster than measured dissociation rates at this energy), the IVR of many states appears to be nearly complete. Few states appear to sample ≤50% of the available vibrational-phase space during this same time period. This is in strong contrast to the mode-specific behavior of HFCO, where many states show little or no evidence for anharmonic mixing of the bright state with background levels, while several levels exhibit state densities that are 4−5 times the symmetry-specific direct count.[10] Most of the HFCO levels with high state densities are $J = 2$, $K_a = 2$ levels, and the state densities are not higher than the rovibrational state densities ($\rho_{rovib} = \rho_{vib}(2J + 1)$). However, a few HFCO 0_{00} levels do have state densities that are at least 2 times the average (over 100 cm^{-1} intervals) symmetry-specific direct count ($\rho_{HFCO}(A') = 2.8/cm^{-1}$ at 15 000 cm^{-1}). This is consistent with the local fluctuations in the calculated state densities ($2\sigma = 3.6/cm^{-1}$ for densities averaged over 1 cm^{-1} intervals) of HFCO A′ states at 15 000 cm^{-1}. Alternatively, the calculated average state densities may underestimate the true state densities by a factor of 2 for HFCO.

Comparison of the clump structure in the A″ states at 15 700.3 (Figure 3) and 15 803.6 cm^{-1} (Figure 13) suggests qualitatively different IVR to the background states. This is not reflected in the state densities of 5.6 and $5.7/cm^{-1}$, however. The dilution factor, discussed by Perry et al.,[38-40] provides additional insight. The dilution factor is defined as $\phi_d = \Sigma I_i^2/(\Sigma I_i)^2$ where I_i are the intensities of the individual lines in a clump. The inverse of the dilution factor is interpreted as the effective number of coupled levels. For two coupled states with equal intensity, $\phi_d = 0.5$ and the effective number of coupled levels is 2. For two coupled lines with an intensity ratio of 3:1, $\phi_d = 0.625$ and the effective number of coupled levels is only 1.6, reflecting weaker coupling. The effective number of coupled levels in these two spectra is 14 ($\phi_d = 0.07$) and 9 ($\phi_d = 0.11$), respectively. It is also apparent that the interaction width is larger for the spectrum in Figure 3. Thus, although the state densities are similar and in both cases less than the symmetry-specific state density, the state at 15 700 cm^{-1} is coupled more strongly to a larger number of background states.

VII. Conclusions

Features in the $2^1 5^1 6^2$ DF spectrum are assigned as strongly coupled members of a 266 polyad of vibrational states. The Franck−Condon active states in these polyads are primarily the zero-order states $2_n 6_m$ with values of n ranging from 0 to 4 and values of m ranging from 13 to 19. The Franck−Condon active states in the $5^1 6^6$ spectrum are more strongly coupled members of the 266 polyad, as evidenced by the significantly more complicated Franck−Condon envelope. The assignment of the Franck−Condon active states is consistent with the HFCO experimental results and Franck−Condon factor calculations.

Multiple IVR time scales are evident in the spectra examined at different resolutions. The fastest IVR results from the low-order 266 resonance that couples the out-of-plane bending vibration and the CO stretching vibration. This resonance acts to distribute the zero-order Franck−Condon factors among the vibrational states comprising the groups of features observed in the $2^1 5^1 6^2$ DF spectrum. This initial IVR occurs in 25 fs, effectively removing the bottleneck to IVR that results in the stability of the extreme-motion out-of-plane bending vibrations in HFCO. Eigenstates of the 266 polyad are then coupled to states with excitation in ν_3 and ν_5 via the 233 and 3566 resonances. This second step is slower (0.5 ps) and results in further dilution of the Franck−Condon factors in the vicinity of a single DF feature. Observed level spacings, both across a group of DF features and under a single feature, are consistent with the calculated spacings of eigenstates in a 266−233−3566 polyad. Clumps of vibrational lines within individual SEP bands indicate further anharmonic and weak A-type Coriolis coupling to background levels at times between 3 and 150 ps. Comparison of the observed and calculated vibrational state densities indicates that, on these time scales, IVR may be nearly complete for many dissociative vibrational states of DFCO. The IVR dynamics of DFCO are in marked contrast to the mode-specific IVR dynamics of HFCO. The quasistability of extreme-motion out-of-plane vibrations in HFCO is destroyed by the presence of the strong low-order resonance between ν_2 and $2\nu_6$ in DFCO.

Multiple time scales were also observed in the IVR dynamics of CH_3OH in the vicinity of the $5\nu_{OH}$ band. The fastest IVR results from a strong, low-order resonance between the OH and CH stretches. Subsequent IVR from the OH/CH stretching vibrations to background levels varies by a factor of 5 in rate over an energy window of only 50 cm^{-1}; this highlights the importance of the density of specific, low-order resonances over the total state density for determining the extent and rate of IVR. Comparison of the HFCO/DFCO and CH_3OH dynamics is striking and emphasizes the importance of specific, low-order resonances in determining intramolecular vibrational dynamics.

Acknowledgment. The National Science Foundation is gratefully acknowledged for their financial support (CHE #9316640). C.B.M. gratefully acknowledges an award from the Alexander von Humboldt Foundation and the generous hospitality of the Max Planck Institute for Quantum Optics. We thank Prof. M. Greubele for a draft of ref 13.

References and Notes

(1) Marcus, R. A. *J. Chem. Phys.* **1952**, *20*, 359.

(2) Forst, W. *Theory of Unimolecular Reactions*; Academic Press: New York, 1973.

(3) Gilbert, R. G.; Smith, S. C. *Theory of Unimolecular and Recombination Reactions*; Blackwell Scientific Publications: Oxford, 1990.

(4) Baer, T.; Hase, W. L. *Unimolecular Reaction Dynamics: Theory and Experiments*; Oxford University Press: Oxford, 1996.

(5) Robinson, P. J.; Holbrook, K. A. *Unimolecular Reactions*; Wiley-Interscience: London, 1972.

(6) Geers, A.; Kappert, J.; Temps, F.; Wiebrecht, J. W. *J. Chem. Phys.* **1994**, *101*, 3634.

(7) Polik, W. F.; Guyer, D. R.; Moore, C. B. *J. Chem. Phys.* **1990**, *92*, 3453.

(8) Polik, W. F.; Guyer, D. R.; Miller, W. H.; Moore, C. B. *J. Chem. Phys* **1990**, *92*, 3471.
(9) Hamilton, C. E.; Kinsey, J. L.; Field, R. W. *Annu. Rev. Phys. Chem.* **1986**, *37*, 493.
(10) Choi, Y. S.; Moore, C. B. *J. Chem. Phys.* **1992**, *97*, 1010.
(11) Crim, F. F. *Science* **1990**, *249*, 1387.
(12) Nesbitt, D. J.; Field, R. W. *J. Phys. Chem.* **1996**, *100*, 12735.
(13) Greubele, M.; Bigwood, R. *Int. Rev. Phys. Chem*,. submitted for publication.
(14) Bethardy, G. A.; Perry, D. S. *J. Chem. Phys.* **1993**, *98*, 6651.
(15) Gambogi, J. E.; Kerstel, E. R. Th.; Lehmann, K. K.; Scoles, G. *J. Chem. Phys.* **1993**, *100*, 2612.
(16) Choi, Y. S.; Moore, C. B. *J. Chem. Phys.* **1991**, *94*, 5414.
(17) Stuchebrukhov, A. A.; Marcus, R. A. *J. Chem. Phys.* **1993**, *98*, 6044.
(18) Lehmann, K. K.; Kerstel, E. R. T.; Lehmann, K. K.; Mentel, T. F.; Pate, B. H. *J. Phys. Chem.* **1991**, *95*, 8282.
(19) Lubich, L.; Boyarkin, O. V.; Settle, R. D. F.; Perry, D. S.; Rizzo, T. R. *Faraday Discuss.* **1995**, *102*, 167.
(20) Hose, G.; Taylor, H. S. *Chem. Phys.* **1984**, *84*, 375.
(21) Crane, J. C.; Kawai, A.; Nam, H.; Clauberg, H.; Beal, H. P.; Guinn, P.; Moore, C. B. *J. Mol. Spectrosc.* **1997**, *183*, 273.
(22) Wei, T. G.; Wyatt, R. E. *J. Phys. Chem.* **1993**, *97*, 13580.
(23) Green, W. H.; Jayatilaka, D.; Willetts, A.; Amos, R. D.; Handy, N. C. *J. Chem. Phys.* **1990**, *93*, 4965.
(24) Yamamoto, T.; Kato, S. *J. Chem. Phys.* **1997**, *107*, 6114.
(25) Budenholzer, F.; Yu, T. *J. Phys. Chem. A* **1998**, *102*, 947.
(26) Goddard, J. D.; Schaefer, H. F., III *J. Chem. Phys.* **1990**, *93*, 4907.
(27) Kamiya, K.; Morokuma, K. *J. Chem. Phys.* **1991**, *94*, 7287.
(28) Francisco, J. S.; Zhao, Y. *J. Chem. Phys.* **1992**, *96*, 7587.
(29) Crane, J. C.; Nam, H.; Beal, H. P.; Clauberg, H.; Choi, Y. S.; Moore, C. B.; Stanton, J. F. *J. Mol. Spectrosc.* **1997**, *181*, 56.
(30) Moore, C. M. *MIT Wavelength Tables*; MIT Press: Cambridge, MA, 1969.
(31) Olah, G. A.; Nojima, M.; Kerekes, I. *Synthesis* **1973**, 487.
(32) Stanton, J. F.; Gauss, J. *Theor. Chim. Acta* **1995**, *91*, 267.
(33) Ikeda, N.; Yamanouchi, K.; Tsuchiya, S.; Jonas, D. M.; Lundberg, J. K.; Adamson, G. W.; Field, R. W. *J. Chem. Phys.* **1991**, *95*, 6330.
(34) Demtroder, W. *Laser Spectroscopy*; Springer-Verlag: New York, 1981.
(35) Beal, H. P. University of California, Berkeley, 1997.
(36) Wilson, E. B., Jr.; Decius, J. C.; Cross, P. C. *Molecular Vibrations*; Dover Publications: New York, 1955.
(37) Guinn, P. L. Ph.D. Thesis, University of California, Berkeley, 1992.
(38) Perry, D. S. *J. Chem. Phys.* **1993**, *98*, 6665.
(39) Go, J.; Perry, D. S. *J. Chem. Phys.* **1995**, *103*, 5194.
(40) Bethardy, G. A.; Perry, D. S.; Davis, M. J.; Go, J. *Faraday Discuss.* **1995**, *102*, 215.